ARTICLE
PUBLISHED ONLINE: 13 FEBRUARY 2011 | DOI: 10.1038/NCHEMBIO.524
nature chemical biology

Structural basis for RNA trimming by RNase T in stable RNA 3′-end maturation

Yu-Yuan Hsiao[1,2], Che-Chuan Yang[2,3], Chia Liang Lin[1,2], Jason L J Lin[2], Yulander Duh[2] & Hanna S Yuan[2,3]*

RNA maturation relies on various exonucleases to remove nucleotides successively from the 5′ or 3′ end of nucleic acids. However, little is known regarding the molecular basis for substrate and cleavage preference of exonucleases. Our biochemical and structural analyses on RNase T–DNA complexes show that the RNase T dimer has an ideal architecture for binding a duplex with a short 3′ overhang to produce a digestion product of a duplex with a 2-nucleotide (nt) or 1-nt 3′ overhang, depending on the composition of the last base pair in the duplex. A 'C-filter' in RNase T screens out the nucleic acids with 3′-terminal cytosines for hydrolysis by inducing a disruptive conformational change at the active site. Our results reveal the general principles and the working mechanism for the final trimming step made by RNase T in the maturation of stable RNA and pave the way for the understanding of other DEDD family exonucleases.

Nucleases are responsible for cleaving phosphodiester bonds between nucleotides in nucleic acids and are crucial for many genetic events, such as DNA replication, recombination and repair, as well as RNA processing, interference and turnover. Endonucleolytic DNases and RNases have been studied extensively, and, as a result, a plethora of information is available on how they select their substrates for site-specific or nonspecific cleavages within a polynucleotide chain. However, little is known regarding the substrate specificity and the cleavage preference of exonucleases, which digest DNA or RNA from the 5′ or 3′ end and remove one nucleotide at a time. Here, using RNase T as a model system, we dissect the structural basis of its substrate specificity and derive general principles for the final trimming process made by RNase T in stable RNA maturation.

RNase T belongs to the DEDD 3′-to-5′ exonuclease superfamily, also referred to as DnaQ-like or RNase D superfamily[1]. The DEDD family proteins, including DEDDh and DEDDy sub-families, all bear four conserved metal-binding acidic residues and one general base residue (histidine or tyrosine) in the active site and share a common two–metal ion mechanism of hydrolysis[2,3]. They are widely spread and have many essential functions in trimming and degrading DNA and RNA in prokaryotes and eukaryotes. Representative members of this family include *Escherichia coli* DNA polymerase III epsilon subunit, an enzyme involved in the proofreading step during DNA replication[3]; yeast Rrp6, which functions in rRNA maturation[4]; *Caenorhabditis elegans* CRN-4, which is involved in the degradation of chromosomal DNA during apoptosis[5]; human PARN, an enzyme that deadenylates poly-A tails in mRNA[6]; and human TREX1, an enzyme contributing to DNA degradation[7,8].

RNase T was first discovered in *E. coli* as an exoRNase involved in transfer RNA (tRNA) turnover and maturation[9]. Subsequently, it was shown to participate in the final trimming of many stable RNAs, including 5S and 23S rRNA, and M1, 10Sa and 4.5S small RNA[10–13]. The mature form of all these stable RNAs has the 5′ end annealed with the 3′ end to generate a duplex structure with a 3′ overhang. Knockout of RNase T resulted in a slow-growth phenotype[14] and a slow recovery from metabolic stress in *E. coli*[15]. It has been shown that RNase T is essential in the maturation of 5S and 23S rRNA, whose precursors are first processed by endoRNase RNase E[16] and RNase III[17], before they are finally trimmed by RNase T[10,12]. RNase T is also an important enzyme in the maturation of tRNA, whose precursors are usually first cleaved by RNase E to result in long 3′ trailer sequences, which are further digested by RNase II, RNase D and/or PNPase to produce a tail with 2–4 extra nucleotides at the 3′ end[18]. A final 3′-terminal trimming of tRNA is subsequently carried out by RNase T and RNase PH[13,19].

Biochemical and crystal structural studies showed that RNase T is a dimeric enzyme and that dimer formation is essential for its activity[20–22]. RNase T has both DNase and RNase activity, preferring DNA over RNA and single-stranded over double-stranded nucleic acids[23,24]. Intriguingly, RNase T has an unusual substrate specificity in digesting single-stranded RNA (ssRNA): a single C residue at the 3′ end reduces its activity by more than 100-fold, whereas the 3′-terminal dinucleotide CC sequence essentially abolishes its enzymatic activity[23,25]. Moreover, double-stranded structures also inhibit the enzymatic activity of RNase T; therefore, a 3′ overhang of a duplex is digested by RNase T near the duplex region[25].

However, a mechanistic understanding of RNase T's substrate specificity and its inhibition by 3′-terminal cytosines and a duplex structure has been lacking. Here we report five crystal structures of RNase T and RNase T in complex with single-stranded and double-stranded DNA (ssDNA and dsDNA). Combined with biochemical, mutational and *in vivo* data, we show that the dimerization of the two RNase T subunits results in a specific architecture that is required for substrate selection and cleavage and report the mechanism for how RNase T screens out 3′-terminal C residues and duplex structures for cleavage. Our studies provide first insights, to our knowledge, into the substrate and cleavage preferences of an exonuclease and shed light on the general principles of the final trimming made by RNase T in stable RNA maturation.

RESULTS

RNase T is blocked by a duplex structure and a 3′-end C

To understand the molecular basis of RNase T in RNA processing, we expressed and purified RNase T for biochemical and structural analysis. The N-terminal His-tagged wild-type dimeric RNase T and a single-point mutant E92G were expressed in *E. coli* and purified to homogeneity by chromatographic methods (see **Supplementary Results** and **Supplementary Fig. 1a**). The E92G mutant was generated accidentally in cloning procedures. It turned out to be a stable mutant showing catalytic behavior (see below) similar to that of wild-type RNase T. RNase T formed a stable dimer with a molecular

[1]Institute of Bioinformatics and Structural Biology, National Tsing Hua University, Hsinchu, Taiwan, ROC. [2]Institute of Molecular Biology, Academia Sinica, Taipei, Taiwan, ROC. [3]Graduate Institute of Biochemistry and Molecular Biology, National Taiwan University, Taipei, Taiwan, ROC. *e-mail: hanna@sinica.edu.tw

weight of ~50 kDa (**Supplementary Fig. 1b**,**c**). We also confirmed that the recombinant RNase T is a 3′-to-5′ exonuclease in digesting ssDNA, that the exposed 3′-OH is required for the nuclease activity and that RNase T binds ssDNA with higher affinity and cleaves ssDNA more efficiently (by at least 20-fold) than dsDNA (**Supplementary Figs. 1d**,**e** and **2a**).

To find out whether RNase T has a sequence specificity in digesting ssDNA, we synthesized ssDNA and ssRNA with different 3′-end sequences for RNase T digestion assays. Substrate-binding and exonuclease activity of RNase T was blocked for both ssRNA and ssDNA by the 3′-terminal C and most strongly by the CC dinucleotide sequence, thus leading to a digestion efficiency in the order AA > AC > CC (**Supplementary Fig. 2b**,**c**). E92G was found to possess nuclease activity and sequence specificity similar to those of wild-type RNase T (**Supplementary Fig. 2d**), suggesting that both enzymes have similar folded structures and catalytic properties. Taken together, these results confirm that RNase T is a 3′-5′ exonuclease and that its exonucleolytic activity is blocked by double-stranded structures and 3′-terminal C residues in digesting RNA and DNA; the two types of blockage are hereafter referred to as 'double-strand effect' and 'C effect'.

RNase T bound with a preferred ssDNA with a 3′-end G

To provide structural insights into RNase T, we determined five crystal structures: (i) apo RNase T (E92G mutant); (ii) a preferred complex RNase T–DNA4: RNase T bound to a 7-nt ssDNA with a preferred 3′-terminal G (only the last four nucleotides TAGG-3′ are visible) and two Mg^{2+} per active site; (iii) a nonpreferred complex RNase T–DNA2: RNase T (E92G mutant) bound to a GC dinucleotide with a nonpreferred 3′-terminal C and a single Mg^{2+} per active site; (iv) a nonpreferred complex RNase T–DNA3: RNase T bound to a 7-nt ssDNA with a nonpreferred 3′-terminal C (with only the last three nucleotides AAC-3′ visible); and (v) a duplex complex RNase T–DNA7**:** RNase T bound to DNA that forms a duplex structure with a 2-nt–long 3′ overhang. The five structures were solved at 2.1–2.3-Å resolutions by molecular replacement using the crystal structure of the wild-type *Pseudomonas aeruginosa* RNase T (PDB ID: 2F96)[22] or the apo *E. coli* RNase T (PDB ID: 3NGY, this study) as the searching model (see **Supplementary Table 1** for the diffraction and refinement statistics of the five structures; crystallization conditions are listed in **Supplementary Table 2**).

The crystal structure of the preferred complex RNase T–DNA4 showed that the two active sites faced opposite sides (see **Fig. 1** and **Supplementary Movie 1).** In this complex, RNase T was bound with a preferred substrate consisting of a 7-nt ssDNA with a 3′-terminal G (5′-TTATAGG-3′; only the last four nucleotides were visible). Similar α/β globular fold and dimeric assembly have been observed in wild-type RNase D and oligoRNase[26,27]. Superposition of the apo RNase T with the substrate-bound RNase T (RNase T–DNA4 complex) gave an r.m.s. deviation of 0.55 Å for 1,608 atoms, suggesting that RNase T retained its conformation after substrate binding. Only the two phenylalanine side chains, Phe29 and Phe146, rotated slightly to make van der Waals interactions with the 3′-terminal guanine bases. The five conserved catalytic residues in the apo RNase T and the preferred RNase T–DNA4 complex, Asp23, Glu25, Asp125, His181 and Asp186, superimpose well with those in TREX1[28], showing that RNase T has a conserved active-site structure as compared to other DEDDh nucleases (**Fig. 1**, right panel).

In the preferred RNase T–DNA4 complex, two well-ordered Mg^{2+} ions are found. Magnesium ion A is coordinated to four ligands: the carboxyl side chain of Asp23, Glu25 and Asp186 and the scissile phosphate; magnesium ion B is coordinated to six ligands in an octahedral geometry: Asp23, two scissile phosphate oxygen atoms and three water molecules. The nucleophilic water molecule that is supposed to be bound between Mg A and His181 is missing in the active site. Because the crystal of the RNase T–DNA4 complex was grown in an acidic solution (pH 6), His181 was protonated and could not bind a nucleophilic water. The RNase T–DNA4 complex was therefore trapped in an active state with only the nucleophilic water missing for hydrolysis.

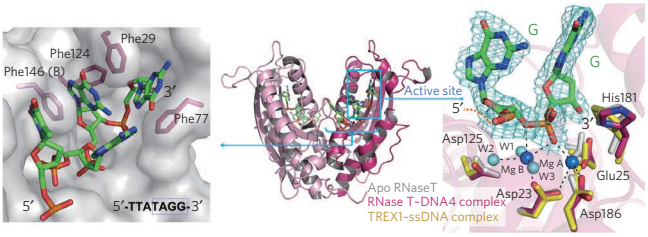

Figure 1 | The crystal structure of the preferred RNase T–DNA complex. The crystal structure of RNase T (one subunit in pink, one in red) in complex with a 7-nt ssDNA (green) with a preferred 3′-terminal G (referred to RNase T–DNA4 complex as only the four last nucleotides are visible: -TAGG-3′). The right panel shows a superposition of the DEDDh active sites of apo RNase T (gray), preferred RNase T–DNA4 complex (red) and TREX1–DNA complex (yellow, PDB ID: 2OA8), along with the 2Fo-Fc electron density of the nucleotide bound in the RNase T–DNA4 complex, contoured at 1.0 σ. Two Mg^{2+} ions (Mg A and Mg B) are bound at the active site of the RNase T–DNA4 complex. The left panel shows that the 3′-terminal sequence (-TAGG-3′) is bound in the narrow groove with Phe29 and Phe77 stacking with the ultimate G and Phe124 and Phe146 stacking with the penultimate G residue. See also **Supplementary Figure 3** and **Supplementary Movie 1**.

The molecular surface of the apo RNase T reveals a deep narrow groove near the DEDD active site, and the RNase T–DNA4 complex structure shows that the last two nucleotides (-TAGG-3′) fit well into this substrate-binding groove (**Fig. 1**, left panel). Four aromatic residues make π-π stacking interactions with the two 3′-terminal bases: Phe29 and Phe77 are stacked with the ultimate G, and Phe124 and Phe146 (B chain) are stacked with the penultimate G (**Supplementary Fig. 3**). These four aromatic residues form a narrow groove suitable for the interaction with single-stranded nucleic acids, explaining the fact that RNase T is specific for ssDNA and ssRNA.

RNase T bound with a nonpreferred ssDNA with a 3′-end C

Why is the exonuclease activity of RNase T blocked by a 3′-terminal C? To answer this question, we determined the crystal structures of RNase T in complex with ssDNA with a nonpreferred 3′-terminal C, DNA2 (GC-3′) and DNA3 (AAC-3′). The superposition of the structures of the preferred RNase T–DNA4 complex with those of nonpreferred RNase T–DNA2 and RNase T–DNA3 complexes shows that the active-site structure of RNase T changed its conformation from an active state to an inactive state upon binding to an oligonucleotide with a 3′-terminal C (see **Fig. 2** and **Supplementary Movie 2**). In the nonpreferred complexes, the side chain of Glu73 (OE1 and OE2) is rotated ~180° to make hydrogen bonds with the 3′-terminal C. The aromatic side chains of Phe29 and Phe27 are also shifted to new positions to stack with the 3′-terminal cytosine; together with Glu73, they pull the cytosine further away from the active site. The α-helix, holding the residues Glu73 and Phe77, functions as a swing that is shifted more than 1 Å upon 3′-terminal C binding (**Fig. 2a**). The loop holding the general base His181 is also shifted away from the active site, and the side chain of His181 is further rotated away from the active site in the nonpreferred RNase T–DNA2 and RNase T–DNA3 complexes than in the preferred complex.

A closer comparison between the preferred RNase T–DNA4 and the nonpreferred RNase T–DNA complexes showed that the scissile phosphate in the nonpreferred complex moves up away from the active site more than in the preferred complex (**Fig. 2a**,**b**). The bound ssDNA with a 3′-terminal C in the nonpreferred RNase

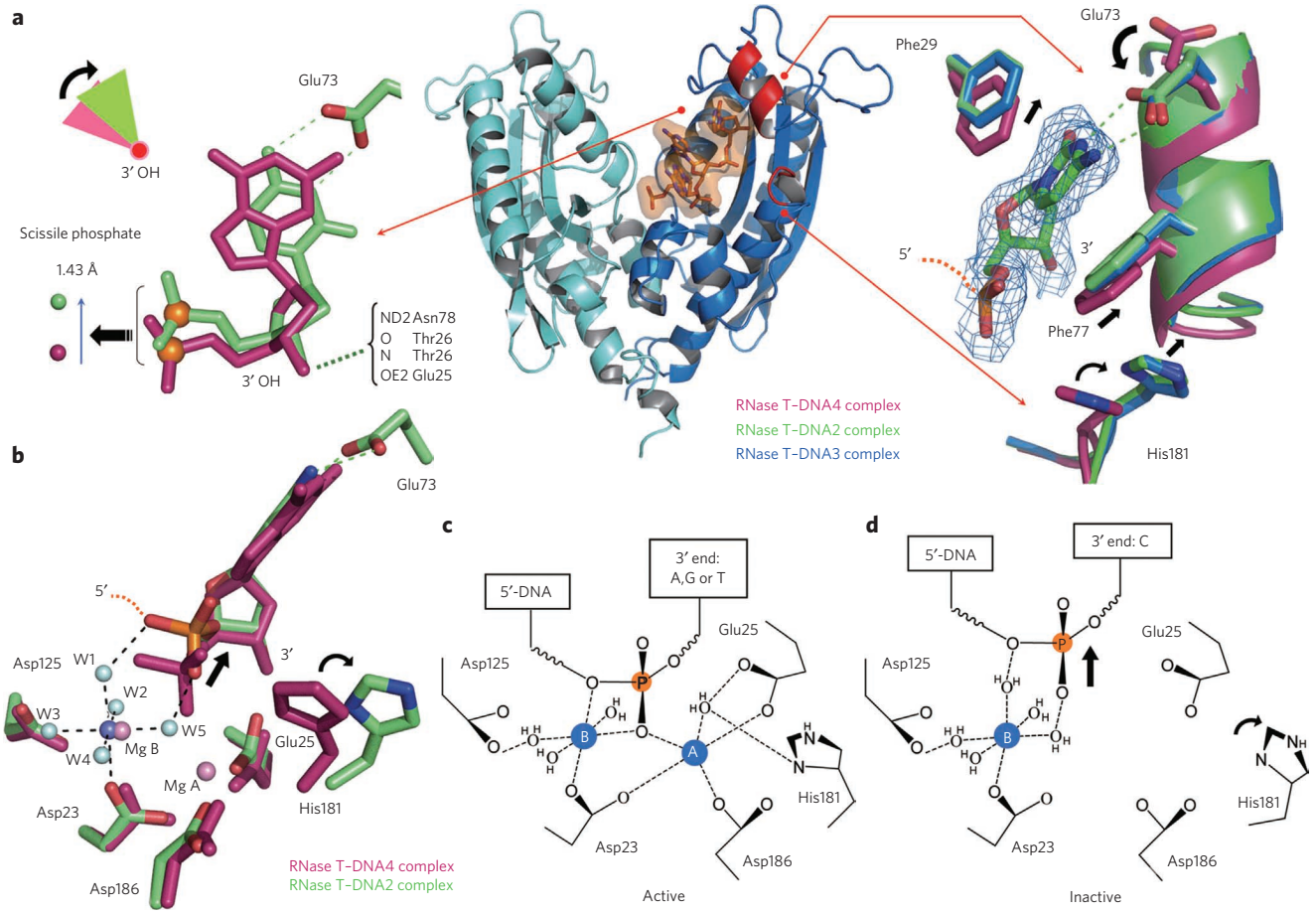

Figure 2 | The crystal structure of the nonpreferred RNase T–DNA complexes. (**a**) The crystal structure of the nonpreferred RNase T–DNA3 complex shows that the binding of a DNA with a nonpreferred 3′-terminal C induces conformational changes in RNase T (shown in red). The right panel shows a close-up view of the three superimposed structures: preferred RNase T–DNA4 complex (red), nonpreferred RNase T–DNA2 (green) and nonpreferred RNase T–DNA3 (blue), along with the 2Fo-Fc electron density of the 3′-C bound in the RNase T–DNA3 complex, contoured at 1.0 σ. The left panel shows a close-up view of the superimposed DNA in the preferred RNase T–DNA4 complex (red) and nonpreferred RNase T–DNA2 (green) complex. The scissile phosphate in the nonpreferred RNase T–DNA2 complex moves up, farther away from the active site. (**b**) Superposition of the active sites of the nonpreferred RNase T–DNA2 complex (green) and the preferred RNase T–DNA4 complex (red). Two metal ions are bound in the preferred complex (pink), and the scissile phosphate is bridged between the two metal ions, whereas only a single metal ion (Mg B, blue) is bound in the nonpreferred complex. (**c**) The schematic diagram of the active conformation in the active site of the preferred RNase T–DNA4 complex. (**d**) The schematic diagram of the inactive conformation in the active site of the nonpreferred RNase T–DNA2 complex. The His181-activated water was adopted from the structure of the TREX1–DNA complex (PDB ID: 2OA8). See also **Supplementary Movie 2**.

T–DNA2 complex is rotated using the 3′-OH as the rotation center to move up the scissile phosphate by 1.43 Å (**Fig. 2a**, left panel). The preferred RNase T–DNA4 complex has an active site in an active conformation with two metal ions bound to four DEDD acidic residues and the His181-activated nucleophilic water molecule located near the scissile phosphate (see **Fig. 2c**). However, in the nonpreferred RNase T–DNA2 complex, the binding of the 3′-terminal C induces a conformational change disrupting the active structure; as a result, only metal ion B is bound and His181 is rotated away from the active center (**Fig. 2d**). In the absence of metal ion A and the nucleophilic water, the ssDNA with a 3′-terminal C can be bound at the active site; however, it cannot be cleaved by RNase T. In summary, the nonpreferred complex structures show clearly that binding of a ssDNA with a 3′-terminal C to RNase T induces a conformational change and disrupts the structure of the active site, therefore resulting in the C effect.

A ‘C-filter’ screens out 3′-end C residues

Judging from the structural analysis of the nonpreferred RNase T–DNA complexes, the five residues Phe29, Glu73, Phe77, Phe124 and Phe146 that interact with the two 3′-terminal bases likely dominate the C effect (see **Fig. 3a**,**b**). The four phenylalanine residues are strictly conserved, and Glu73 is highly conserved in RNase T homologs. To determine the contribution of these residues to the C effect, we made single point mutant E73A, double mutant F124A/F146A and triple mutant E73A/F29A/F77A. In the double mutant F124A/F146A, the two replaced residues are involved in the binding of the second-to-last A (-AC-3′), whereas in the triple mutant E73A/F29A/F77A, the three replaced residues are involved in the binding of the 3′-terminal C (-AC-3′) in the inactive RNase T–DNA3 complex. DNA digestion assays showed that E73A had reduced exonuclease activity compared with wild-type RNase T (**Fig. 3c**,**d**). Wild-type RNase T and the E73A mutant were further incubated with ssDNA with C nucleotides in the middle of the strand. The cleavage pattern generated from E73A showed less accumulation in the centrally cytosine-containing regions than with wild-type RNase T (**Fig. 3c**). Therefore, E73A had reduced exonuclease activity and reduced sequence specificity as compared to those of wild-type RNase T. The nitrocellulose filter binding assay, however, showed that E73A bound ssDNA with a similar affinity

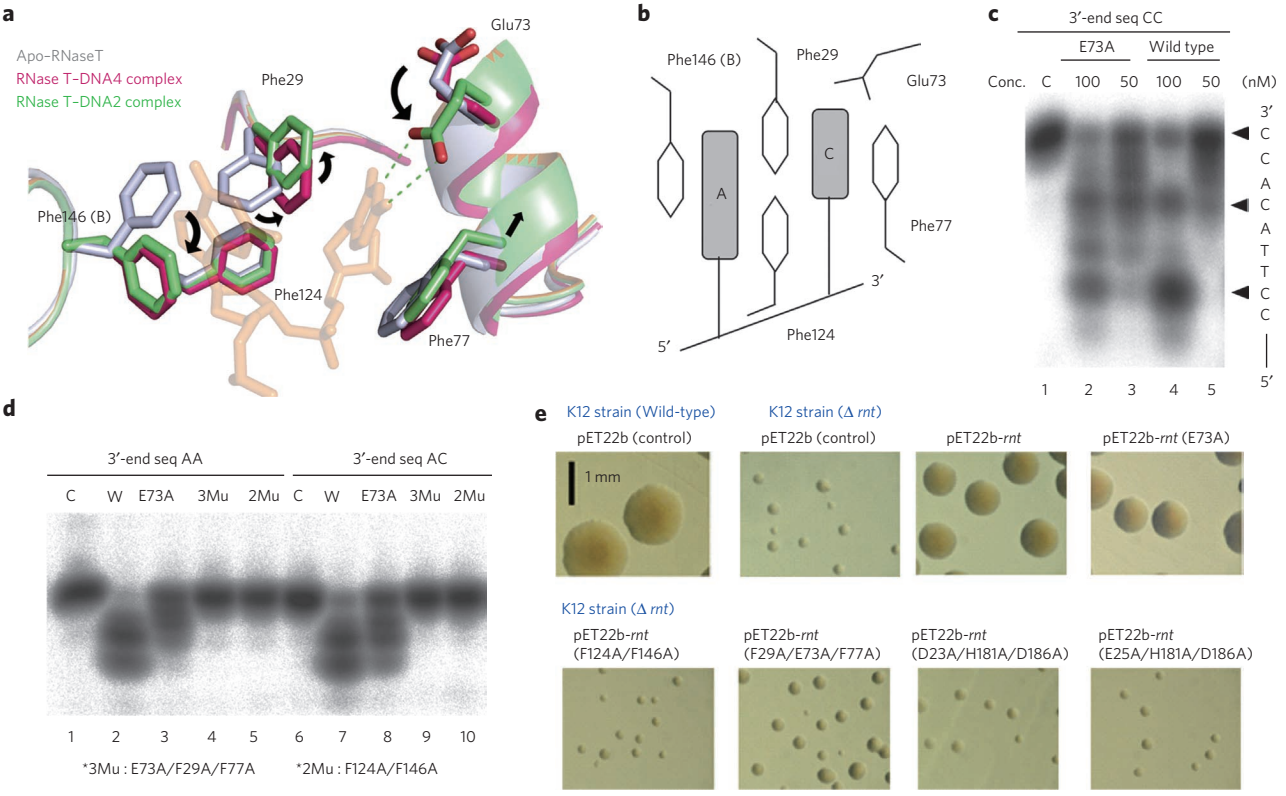

Figure 3 | A C-filter in RNase T deselects DNA with a 3′-terminal C for cleavage. (**a**,**b**) The structure and schematic diagram of the five amino acids—Phe29, Glu73, Phe77, Phe124 and Phe146—involved in binding to the 3′-terminal nucleotides in the RNase T. The side chains of Phe29 and Phe146 rotated the most to interact with the two 3′-terminal bases in the nonpreferred RNase T–DNA2 complex. (**c**) The RNase T mutant E73A accumulated fewer cleavage products at the regions containing internal cytosines as compared to wild type. (**d**) The nuclease activity assays of wild-type and mutated RNase T. E73A had reduced nuclease activity, whereas the triple (E73A/F29A/F77A) and double (F124A/F146A) mutants had no activity. (**e**) Colony size variations of *E. coli* wild-type and mutant K12 strains on LB plates show that the RNase T deletion strain (Δ*rnt*) had a slow-growth phenotype that can be almost fully rescued by introducing a plasmid containing wild-type RNase T or mutant E73A but cannot be rescued (or can be only slightly rescued) by the plasmid encoding the double mutant F124A/F146A and the triple mutants D23A/H181A/D186A, D23A/H181A/D186A and E73A/F29A/E77A. See also **Supplementary Figure 4**.

as wild-type RNase T, indicating that the reduced exonuclease activity and reduced sequence specificity was not caused by reduced substrate binding (**Supplementary Fig. 4a–c**). These results suggest that Glu73 is involved in directing the C effect but is not the only such residue. In contrast to E73A, the double and triple mutants almost completely lost their exonuclease activity (**Fig. 3d**, lanes 4, 5, 9 and 10). The filter-binding assays further showed that the double mutant and triple mutant had much reduced DNA-binding affinity (**Supplementary Fig. 4c**). Moreover, the double mutant F124A/F146A had higher binding affinity for -AA-3′ than -AC-3′, suggesting that the 3′-terminal C was less favored, as screened by Phe29, Glu73 and Phe77. Similarly, the triple mutant E73A/F29A/F77A bound -AC-3′ more tightly than -CC-3′, suggesting that a C located at the penultimate position was less favored, as screened by Phe124 and Phe146.

To test whether these residues are also required for the normal function of RNase T *in vivo*, transformation rescue experiment were carried out in the *rnt*-deletion strain (K12 strain Δ*rnt*) by introducing a construct expressing the mutant of RNase T (see **Fig. 3e** and **Supplementary Fig. 4d**). The *rnt*-deletion strains had a severe slow-growth phenotype, which was almost fully rescued by the wild-type *rnt* and the single mutant E73A. However, the double (F124A/F146A) and the triple mutants (F29A/E73A/F77A), as well as the two active site mutants (D23A/H181A/D186A and E25A/H181A/D186A), either did not rescue or only slightly rescued the slow-growth defect. These results, which are consistent with the biochemical assays, show that the four aromatic residues (Phe29, Phe77, Phe124 and Phe146) in RNase T play critical roles for the normal trimming activity in bacterial cells. Combining the structural, biochemical and *in vivo* data, we show here that the C effect of RNase T results not only from a conformational change but also from poor interactions between phenylalanine residues and cytosine bases at the two 3′-terminal positions. Statistical analyses of RNA-binding proteins showed that the aromatic side chain of phenylalanine stacks frequently with A, U and G but seldom with C, suggesting that phenylalanine does not favorably interact with a cytosine[29–31]. We therefore conclude that the five residues Glu73, Phe29, Phe77, Phe124 and Phe146 form a C-filter to deselect C, thus leading to a C effect in RNase T.

RNase T is ideal for binding a duplex with a 3′ overhang

Most of the natural RNA substrates of RNase T, such as tRNA and rRNA precursors, have a double-stranded duplex structure with a 3′ overhang; however, it was unclear how RNase T binds and digests a 3′-overhang duplex structure. To provide structural insights into the role of RNase T in RNA maturation, we also crystallized RNase T with a DNA duplex containing a 2-nt 3′ overhang (RNase T–DNA7 complex in **Supplementary Table 1**). In this complex, the 7mer DNA (5′-TTACAAC-3′) annealed into a double-stranded structure with a 2-nt 3′ overhang because the duplex DNA structure was favored under the more neutral (pH 5.5) crystallization condition as compared to the acidic crystallization condition (pH 3.5) of the RNase T–DNA3 complex. The RNase T–DNA7 complex was crystallized

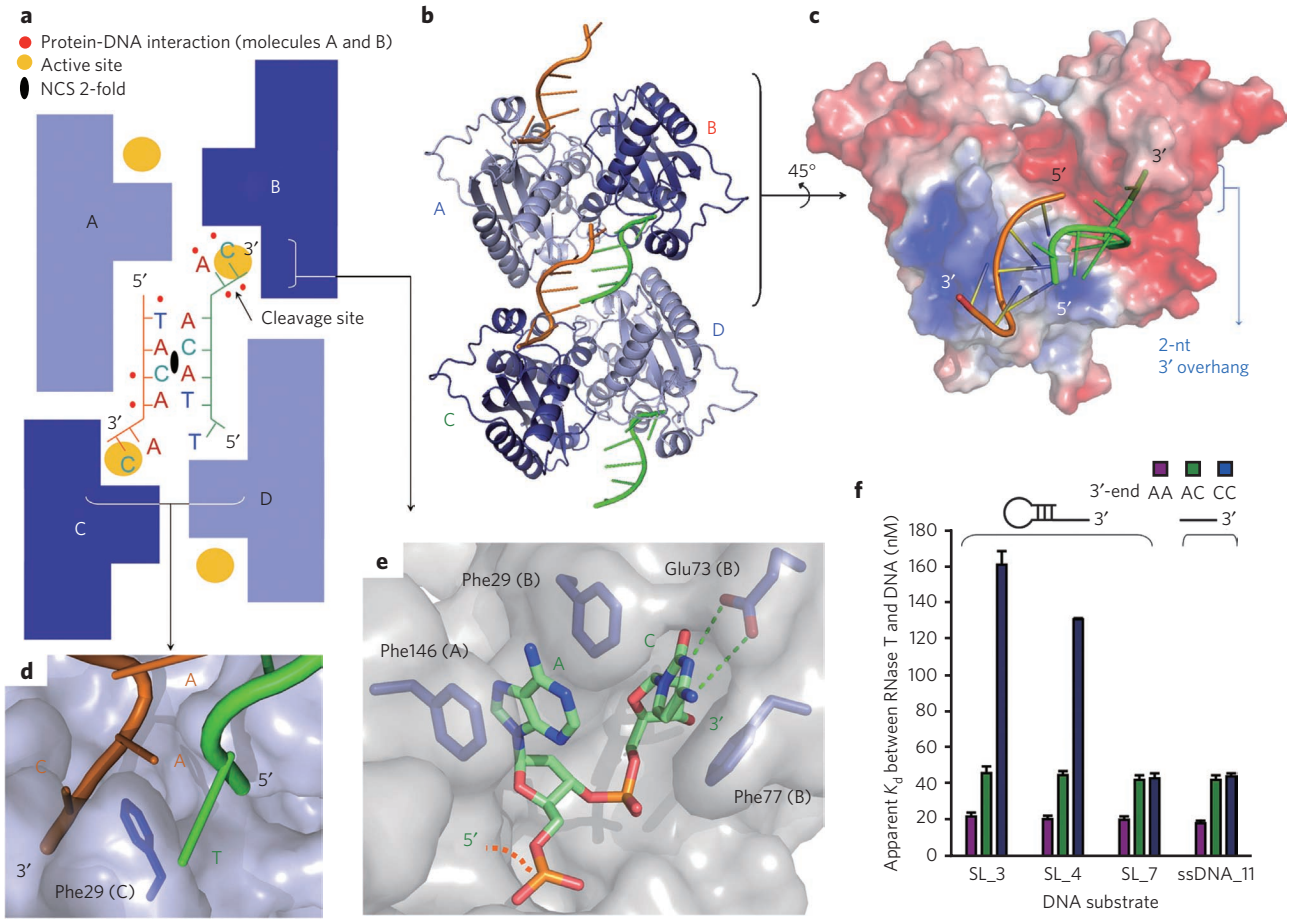

Figure 4 | Crystal structure of RNase T in complex with a duplex DNA with a 2-nt 3′ overhang. (**a**) Schematic diagram of the two RNase T dimers (A-B dimer and C-D dimer) bound to a double-stranded duplex with a 2-nt 3′ overhang. (**b**) The overall crystal structure of RNase T–DNA7 complex in one asymmetric unit. (**c**) The surface electrostatic potential of RNase T shows that the subunit B has a basic region appropriate for binding one DNA strand in the stem structure. Red, –5.0 k_BT/e; blue, +5.0 k_BT/e. k_B, Boltzmann constant; T, temperature in Kelvin; e, charge of an electron. (**d**) The last A-T base pairs at the stem region are melted by stacking with Phe29. (**e**) A close-up view showing that Glu73 makes hydrogen bonds with the 3′-terminal C and the last two bases interact with phenylalanine residues. (**f**) The bar diagram shows the apparent K_d between RNase T and ssDNA and between RNase T and duplex DNAs with different 3′ overhangs. A 3′-terminal dinucleotide CC sequence in the 3′ overhang of a duplex reduces the binding affinity substantially. See also **Supplementary Figures 5** and **6**.

in the low symmetry P1 space group with four RNase T monomers and four strands of 7-nt DNA per asymmetric unit (**Fig. 4**). A noncrystallographic twofold symmetry axis is located in the center of the DNA duplex; as a result, the interactions of the 3′-end duplex with the A-B dimer are almost identical to the ones of the other end of the duplex with the C-D dimer (**Fig. 4a**,**b**). The dsDNA duplex in the complex adopts a B-form conformation as analyzed by CURVES+[32]. For clarity, we describe only the structure of the A and B subunits of the RNase T dimer, which are found to bind to two DNA strands, as C and D subunits share a similar structure to that of A and B subunits (see **Supplementary Fig. 5**).

The structure of the RNase T–DNA7 complex reveals how RNase T binds to a double-stranded duplex structure with a 3′ overhang. Each subunit of the RNase T dimer binds mainly to one strand of DNA. The calculation of the electrostatic surface potential showed that the surface of monomer A is basic and thus suitable for nucleic acid binding (**Fig. 4c**). Most of the interactions between the protein and the DNA duplex region were between protein side chains and the DNA phosphate backbones, suggesting that RNase T has low sequence specificity in connection with the double-stranded region. In summary, the architecture of the dimeric RNase T is ideal for binding a duplex with a short 3′ overhang, with one protomer interacting with the nonscissile strand of the duplex region primarily through electrostatic interactions and the other protomer interacting more strongly with the scissile strand at the 3′-terminal end through π–π stacking and hydrogen bonding.

Trimming of the 3′ overhang of a duplex by RNase T

The 2-nt 3′ overhang is deeply buried in the narrow active site of RNase T (see **Fig. 4e**). This result strongly suggests that an overhang length of at least 2 nt is required for binding and hydrolysis in the narrow active site and that a duplex with only a 1-nt overhang or a blunt end should be a poor substrate for RNase T. We found that RNase T binds with the highest affinity to structures with an overhang ranging from 3 to 7 nt, as measured by the nitrocellulose filter-binding assay (see **Fig. 5a** and **Supplementary Fig. 6c**). On the contrary, a duplex with a 2-nt 3′ overhang bound RNase T less well (about six-fold reduction) and a duplex with a 1-nt overhang or with a blunt end bound RNase T most weakly (about a 1,000-fold reduction). This result suggests that RNase T prefers to bind a duplex with a 3′ overhang with a length of more than 3 nt.

In agreement with the binding results, DNA digestion assays further showed that DNA duplex containing a blunt end and a 1-nt 3′ overhang cannot be cleaved by RNase T (**Fig. 5b**). DNA with a 2-nt 3′ overhang was also not efficiently trimmed by RNase T (the duplex with a 1-nt overhang was produced only at a high enzyme

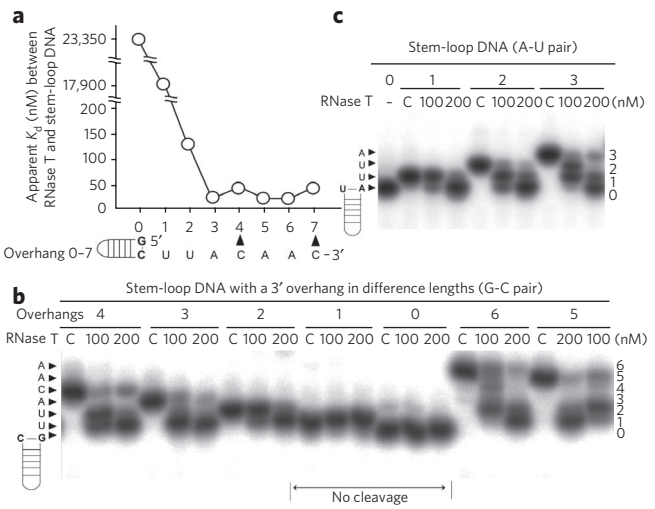

Figure 5 | RNase T cleaves a 3′ overhang duplex to produce a duplex with a 1- or 2-nt 3′ overhang. (**a**) The diagram of apparent dissociation constants (K_d) between RNase T and stem-loop DNA versus the length of overhangs. The stem-loop DNA oligomer has a sequence of 5′-GGCCCUCUUUAGGGCC-overhang-3′. We used dU to replace dT in the sequence. (**b**) Nuclease activity assays of RNase T in digesting the stem-loop DNA with 3′ overhangs of different lengths. The last base pair in the duplex region was a G-C base pair. The duplex with a 0-nt and 1-nt overhang cannot be cleaved by RNase T (200 nM). The duplexes with a 2- to 6-nt overhang were cleaved to a 2-nt or 1-nt overhang depending on the concentration of RNase T. (**c**) When the last base pair in the duplex region was changed to an A-U base pair, the overhangs were cleaved nearer the duplex region to generate products with a 1-nt overhang or no overhang. See also **Supplementary Figures 6** and **7**.

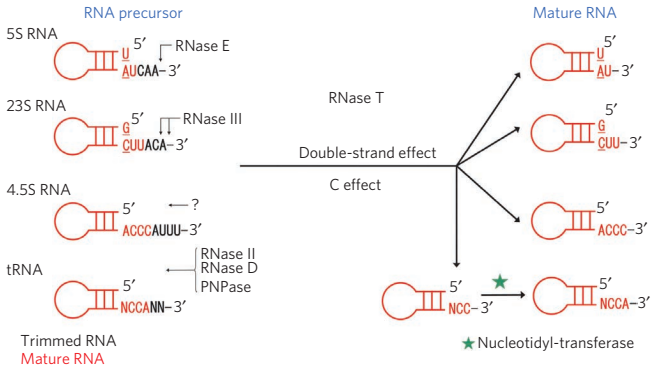

Figure 6 | General principles of the 3′-terminal final trimming made by RNase T in RNA maturation. Ribosomal 5S and 23S RNA are cleaved by RNase T closely to the double-strand region; we propose that the cleavage is mainly regulated by the double-strand effect. The 5S rRNA has an A-U base pair at the end of the duplex, resulting in a 1-nt overhang, whereas the 23S rRNA has a G-C base pair at the end of the duplex, resulting in a 2-nt overhang. Conversely, cleavage of tRNA and 4.5S RNA by RNase T is regulated mainly by the C effect. Cleavage is abolished when RNase T encounters a short repeat (di- or trinucleotide) of cytosines in the 3′ overhang.

concentration of 200 nM). The duplex DNA substrates with longer 3′ overhangs (3–6 nt) were digested to the corresponding products with 2-nt overhangs (or 1-nt overhangs at a high enzyme concentration).

However, the mature 5S and 23S rRNA have either a 1-nt and a 2-nt 3′ overhang, respectively. Why does the final trimming step carried out by RNase T generate overhangs of different lengths in ribosomal RNA? A closer look at the RNase T–DNA7 complex revealed that the last A-T base pair at the end of the double-stranded region had melted; separation and stacking of these bases with Phe29 released more ssDNA for hydrolysis (see **Fig. 4d**). The stem-loop DNA substrates used in the binding and digestion assays possessed a terminal G-C base pair (see **Fig. 5b**), which was less easily melted as compared to an A-U (or A-T) base pair. We therefore hypothesized that a 3′-overhang duplex with an A-U base pair at the end of the duplex region can be cleaved closer to the duplex region. To test whether the cleavage product varies with the composition of the base pair at the end of the duplex regions, we replaced the G-C pair at this position with a dA-dU base pair. Indeed, incubation of these DNA substrates with RNase T led to cleavage nearer the duplex region: at an enzyme concentration of 100 nM, the product with a 1-nt 3′ overhang was primarily generated, whereas at increased RNase T concentration (200 nM) predominantly blunt-ended DNA was obtained (see **Fig. 5c**). We thus conclude that the last base pair in the duplex region affects the final trimming by RNase T. A duplex carrying a 3′ overhang is trimmed by RNase T primarily to a duplex with a 2-nt overhang if G-C is the last base pair or to a duplex with a 1-nt overhang if A-T is the last base pair in the duplex region.

The 3′-end CC induces the C effect for a duplex substrate

We noticed that the side chain of Glu73 in the duplex RNase T–DNA7 complex rotated to make hydrogen bonds with the 3′-terminal C (see **Fig. 4e**); however, the scissile phosphate did not move away from the active site (see **Supplementary Fig. 5a**,**b**). This result suggests that a single 3′-terminal C at the 3′ overhang near the duplex is not sufficient to induce the disruptive conformational change in RNase T. To further reveal the sequence preference of RNase T to double-stranded substrates, we incubated RNase T with duplex DNA carrying various 3′ overhangs. We found that a 3′-terminal CC dinucleotide sequence in a short 3-nt or 4-nt overhang reduced significantly the binding affinity between RNase T and DNA (see **Fig. 4f** and **Supplementary Fig. 6d**). By contrast, with a ssDNA substrate, both a 3′ C and a 3′ CC reduced the binding affinity to a similar extent. Taken together with the structural data, these results suggest that a 3′-terminal C in a ssDNA is sufficient to induce the C effect, whereas a 3′-terminal CC dinucleotide sequence in a duplex with a short 3′ overhang is required to inhibit the activity of RNase T.

DISCUSSION

Previous studies suggest that the natural substrates for RNase T consist exclusively of RNA duplexes containing short 3′ overhangs[10,12,13,19]. The crystal structure of the duplex RNase T–DNA7 complex mimics the structure of RNase T bound with a natural duplex substrate with a 3′ overhang. We found that in this complex Glu73 rotated its side chain to interact with the 3′-terminal C but that the scissile phosphate did not shift away from the active site (**Fig. 4e** and **Supplementary Fig. 6a**), suggesting that a single 3′-terminal C near the duplex structure cannot fully induce the C effect to block the activity of RNase T. In fact, a 3′-terminal dinucleotide CC sequence in the overhang is required to induce the C effect in RNase T, as supported by three lines of evidence. First, a duplex with a 3′ CC overhang had a significantly reduced binding affinity to RNase T as compared to a duplex with a 3′ C overhang (**Fig. 4f**). Second, the DNA digestion experiment showed that a duplex DNA with a single C in the 3′ overhang near the duplex region (SL-UUAC) did not inhibit the enzymatic activity of RNase T (**Fig. 5b**). Third, mutation of the residues involved in the interaction with the penultimate C (F124A/F146A) led to more severe defects in cell growth than mutation of the residues involved in the interaction with the 3′-terminal C (E73A/F29A/F77A) (**Fig. 3e**). All these results support the conclusion that the penultimate C is important in causing the C effect in double-stranded substrates with a short 3′ overhang.

We also found that shortening the 3′ overhang of a duplex to less than 3 nt greatly weakens its association with the enzyme, and thus RNase T products are typically duplexes with 3′ overhangs of 1 to 3 nt. How can we implicate these results in the RNA trimming process undertaken by RNase T in stable RNA maturation? RNase T is essential for the maturation of 5S and 23S rRNA whose 3′ and 5′ ends are annealed to produce a duplex with short 1–2-nt 3′ overhangs (see **Fig. 6**). The 5S rRNA precursors, which were processed by RNase E to intermediates with a 4-nt 3′ overhang, are further trimmed by RNase T to produce the mature 5S rRNA with a 1-nt 3′ overhang[16,33,34]. Similarly, the 23S rRNA precursors represent intermediates with a 4–5-nt 3′ overhang, as a result of RNase III processing[17]; these intermediates are trimmed by RNase T to produce the mature 23S rRNA with a 2-nt 3′ overhang[10,12]. Our studies suggest that the final trimming step of 5S rRNA and 23S rRNA made by RNase T is controlled by the double-strand effect and C effect: the mature 5S rRNA has a 1-nt 3′ overhang owing to the presence of an A-U base pair at the end of the duplex region, whereas the mature 23S rRNA has a 2-nt 3′ overhang because it contains a G-C base pair at this position (see **Fig. 6**). The single C in the overhang region of 5S and 23S RNA intermediates is not sufficient to block the activity of RNase T and is therefore removed by RNase T.

With regard to the maturation of tRNA and other small stable RNA, the final 3′-end trimming made by RNase T is regulated mainly by the C effect on a duplex with a 3′ overhang (that is, the dinucleotide CC effect) as these duplex RNAs carry 3′ overhangs with di- and trinucleotide sequences of cytosines. Our structural analysis strongly supports the model that RNase T trims tRNA up to CC-3′ and the overtrimmed tRNA is subsequently modified by addition of a 3′-terminal A, a reaction catalyzed by tRNA nucleotidyltransferase (CCA-adding enzyme)[35,36]. Similarly, for the trimming of small stable RNA, including 4.5S, M1 and 10Sa, RNase T is likely also controlled by the C effect. The mature 4.5S RNA has a trinucleotide CCC sequence in the 3′-terminal region that should inhibit the activity of RNase T once it encounters this repeat. The mature M1 RNA and 10Sa RNA end with –CCX-3′ (X = A or U), which suggests that they might first be cleaved by an endonuclease, such as RNase E for M1 RNA[37–39], before trimming by RNase T, resulting in a terminal CC sequence. The terminal A or U residue could result from further addition by nucleotidyltransferase, in a way similar to the 3′-end maturation of tRNA. In summary, our structural studies reveal the general principles of RNase T in applying the double-strand effect and the C effect on miscellaneous stable RNA for the generation of mature RNA with correct 3′ overhang sequences.

RNase T not only binds DNA with higher affinity than RNA but also has higher nuclease activity (>10-fold) in digesting DNA as compared to RNA, as shown in a previous and this study. It should be noted that all the substrates in our RNase T complex structures are ss- or dsDNA, and therefore the interactions we derived from the structural studies were extrapolated from DNA to RNA substrates. As an RNA duplex has an A-form–like structure, it likely binds RNase T slightly differently from a DNA duplex with a B-form structure. Nevertheless, upon consideration of the tight binding between RNase T and DNA, it is intriguing to speculate whether cellular DNAs carrying a 3′ overhang could also be natural substrates for RNase T. Several lines of evidence support this possibility. First, many DEDD nucleases cleave primarily DNA rather than RNA, such as *E. coli* DNA polymerase III epsilon subunit and human TREX1[3,40], indicating that RNase T might also target DNA. Second, it has been shown that RNase T affects growth and recovery from metabolic stress and that cells harboring a high copy number of the RNase T gene (*rnt*) have a ~40-fold increased UV survival frequency, suggesting that RNase T may be involved in end-trimming reactions during DNA recombination and/or DNA repair[15,41]. We hypothesize that the identification of DNA substrates for RNase T in *E. coli* would not only reveal the function of RNase T in bacteria but also have implication for the diverse functions of DEDD family nucleases in eukaryotes.

In conclusion, our structural studies of RNase T reveal the underlying working mechanism of this enzyme in substrate selection and digestion. As many DEDD nucleases share a fold and a conserved active site similar to that of RNase T, the structural insight into RNase T not only shows the link between the DEDD domain arrangement and substrate specificity but will aid in understanding the exonuclease activity and identifying possible substrates of other DEDD family proteins, some of which have been linked directly to human diseases, such as WRN in Werner syndrome[42] and TREX1 in Aicardi-Goutieres syndrome and familial chilblain lupus[43,44].

METHODS

Protein expression and purification. The full-length *rnt* gene was amplified by PCR using *E. coli* genomic DNA from JM109 strain and cloned into NdeI/XhoI sites of expression vectors pET-28a (Novagen) to generate the N-terminal His-tagged fused RNase T. The plasmid of pET28–RNase T was transformed into *E. coli* BL21-CodonPlus(DE3)-RIPL strain (Stratagene) cultured in LB medium supplemented with 35 μg ml^{-1} kanamycin. Cells were grown to an optical density of 0.5–0.6 measured at a wavelength of 600 nm and induced by 1 mM IPTG at 18 °C for 20 h. The harvested cells were disrupted by a microfluidizer in 50 mM Tris-HCl (pH 7.5) containing 300 mM NaCl, and the cell extracts were passed through a Ni-NTA resin affinity column (Qiagen Inc.) using a standard protocol. The protein sample was then applied to a HiTrap Heparin column (GE Healthcare) and, subsequently, to a gel filtration chromatography column (Superdex 75, GE Healthcare). Purified RNase T samples were concentrated to 25–35 mg ml^{-1} in 300 mM NaCl and 50 mM Tris-HCl (pH 7.0). RNase T point mutants were generated by using the QuikChange site-directed mutagenesis kit (Stratagene) and purified by the same procedures as those of wild-type RNase T.

DNase and RNase activity assays. DNA and RNA oligonucleotides used for nuclease activity assays were labeled at the 5′ end with [γ-^{32}P]ATP by T4 polynucleotide kinase and at the 3′ end with [α-^{32}P]dCTP by terminal deoxynucleotidyl transferase. The isotope-labeled substrates were purified on a Microspin G-25 column (GE Healthcare) to remove the unincorporated nucleotides. Purified substrates (20 nM; see **Supplementary Table 2** for sequences) were incubated with RNase T or mutants at various concentrations in a buffer solution of 120 mM NaCl, 2 mM $MgCl_2$ and 50 mM Tris-HCl (pH 7.0) at room temperature for 20–60 min. The reaction was quenched by the addition of the stop solution (2× Tris-Borate-EDTA buffer) and heating at 95 °C for 5 min. Reaction samples were then resolved on 20% denaturing polyacrylamide gels and visualized by autoradiography (Fujifilm, FLA-5000).

DNA binding assays. The DNA binding affinity of RNase T was measured with nitrocellulose filter binding assays[45]. A 5′-end ^{32}P-labeled ssDNA substrate (66 pM) was incubated with RNase T or mutants in a solution of 100 mM NaCl, 10 mM EDTA and 50 mM Tris-HCl (pH 7.0) for 25 min at room temperature. The concentrations of the RNase T used in the assays varied from 4.0 to 0.0 μM; 16 different concentrations were used (see **Fig. 3** and **Supplementary Fig. 4**). For low affinity mutants, F124A/F146A and F29A/E73A/F77A, higher protein concentrations (8 and 16 μM) were used. The protein–DNA complex solutions were passed through a filter-binding assay apparatus (Bio-Dot SF microfiltration apparatus, Bio-Rad). The isotope signal from protein–DNA complex bound on the nitrocellulose membrane and the free DNA passed through the filter-binding assay apparatus were exposed to a phosphorimaging plate and visualized by autoradiography (Fujifilm, FLA-5000). The intensities were quantified using the program AlphaImager IS-2200 (Alpha Innotech), and binding percentages from three measurements were calculated to derive the apparent K_d between RNase T and DNA by a one-site binding-curve fitting with GraphPad Prism 4 using the equation of $y = x/(K_d + x)$, where x is the protein concentration and y is the percentage of bound DNA out of total DNA.

Transformation rescue experiments. Wild-type *E. coli* K-12 and RNase T knockout (Δ*rnt*) strains used in the transformation rescue experiments were from the Keio collection[46]. Wild-type and mutant *rnt* genes were cloned into NdeI/XhoI sites of expression vectors pET-22b (Novagen) to generate the plasmids encoding RNase T and mutants under the control of the T7 promoter, which can be induced weakly by *E. coli* RNA polymerase. The constructed plasmids were transformed into *E. coli* K12 wild-type or RNase T knockout strain (Δ*rnt*) and cultured in LB medium supplemented with 100 μg ml^{-1} ampicillin and/or 35 μg ml^{-1} kanamycin. Overnight cultures were diluted 100-fold into 20 ml LB medium and further grown on a rotary shaker (200 r.p.m.) at 37 °C for the measurement of absorption at 600 nm in 30 min intervals.

Crystallization and crystal structural determination. Wild-type RNase T (25–35 mg ml^{-1}) and E92G (20–25 mg ml^{-1}) in 300 mM NaCl and 50 mM Tris-HCl (pH 7.0) were mixed with different ssDNA substrates in the molar ratio of 1:1.2. Detailed information regarding DNA sequences and crystallization conditions of the five structures are given in **Supplementary Table 2**. All crystals were cryo-protected by Paraton-N (Hampton Research) for the data collection at 100 K. X-ray diffraction data of apo RNase T, RNase T–DNA3, RNase T–DNA4 and RNase T–DNA7

complexes were collected at the BL-13B1 at the National Synchrotron Radiation Research Center, Taiwan, whereas the diffraction data of RNase T–DNA2 complex were collected at the BL44XU beamline at SPring-8, Japan. All diffraction data were processed by HKL2000, and the diffraction statistics are listed in **Supplementary Table 1**. Structures were solved by the molecular replacement method using the crystal structure of *Pseudomonas aeruginosa* RNase T (PDB ID: 2F96, chain A) or *E. coli* RNase T (PDB ID: 3NGY, this study) as the search model by program MOLREP of CCP4. The models were built by Coot and refined by Phenix.

Accession codes. Structural coordinates and diffraction structure factors have been deposited in the Protein Data Bank with the PDB ID codes of 3NGY for apo RNase T, 3NH1 for the active RNase T–DNA4 complex, 3NGZ for the inactive RNase T–DNA2 complex, 3NH0 for the inactive RNase T–DNA3 complex and 3NH2 for the duplex RNase T–DNA7 complex.

Received 24 September 2010; accepted 7 January 2011; published online 13 February 2011

References

1. Zuo, Y. & Deutscher, M.P. Exoribonuclease superfamilies: structural analysis and phylogenetic distribution. *Nucleic Acids Res.* **29**, 1017–1026 (2001).
2. Steitz, T.A. & Steitz, J.A. A general two-metal-ion mechanism for catalytic RNA. *Proc. Natl. Acad. Sci. USA* **90**, 6498–6502 (1993).
3. Hamdan, S., Carr, P.D., Brown, S.E., Ollis, D.L. & Dixon, N.E. Structural basis for proofreading during replication of the *Escherichia coli* chromosome. *Structure* **10**, 535–546 (2002).
4. Briggs, M.W., Burkard, K.T. & Butler, J.S. Rrp6p, the yeast homologue of the human PM-Scl 100-kDa autoantigen, is essential for efficient 5.8 S rRNA 3′ end formation. *J. Biol. Chem.* **273**, 13255–13263 (1998).
5. Hsiao, Y.Y. *et al.* Crystal structure of CRN-4: implications for domain function in apoptotic DNA degradation. *Mol. Cell. Biol.* **29**, 448–457 (2009).
6. Wu, M. *et al.* Structural insight into poly(A) binding and catalytic mechanism of human PARN. *EMBO J.* **24**, 4082–4093 (2005).
7. Kavanagh, D. *et al.* New roles for the major human 3′-5′ exonuclease TREX1 in human disease. *Cell Cycle* **7**, 1718–1725 (2008).
8. Crow, Y.J. & Rehwinkel, J. Aicardi-Goutieres syndrome and related phenotypes: linking nucleic acid metabolism with autoimmunity. *Hum. Mol. Genet.* **18**, R130–R136 (2009).
9. Deutscher, M.P., Marlor, C.W. & Zaniewski, R. Ribonuclease T: new exoribonuclease possibly involved in end-turnover of tRNA. *Proc. Natl. Acad. Sci. USA* **81**, 4290–4293 (1984).
10. Li, Z. & Deutscher, M.P. The tRNA processing enzyme RNase T is essential for maturation of 5S RNA. *Proc. Natl. Acad. Sci. USA* **92**, 6883–6886 (1995).
11. Li, Z., Pandit, S. & Deutscher, M.P. 3′ exoribonucleolytic trimming is a common feature of the maturation of small, stable RNAs in *Escherichia coli*. *Proc. Natl. Acad. Sci. USA* **95**, 2856–2861 (1998).
12. Li, Z., Pandit, S. & Deutscher, M.P. Maturation of 23S ribosomal RNA requires the exoribonuclease RNase T. *RNA* **5**, 139–146 (1999).
13. Li, Z. & Deutscher, M.P. Maturation pathways for *E. coli* tRNA precursors: a random multienzyme process in vivo. *Cell* **86**, 503–512 (1996).
14. Kelly, K.O. & Deutscher, M.P. The presence of only one of five exoribonucleases is sufficient to support the growth of *Escherichia coli*. *J. Bacteriol.* **174**, 6682–6684 (1992).
15. Viswanathan, M., Lanjuin, A. & Lovett, S.T. Identification of RNase T as a high-copy suppressor of the UV sensitivity associated with single-strand DNA exonuclease deficiency in *Escherichia coli*. *Genetics* **151**, 929–934 (1999).
16. Misra, T.K. & Apirion, D. RNase E, an RNA processing enzyme from *Escherichia coli*. *J. Biol. Chem.* **254**, 11154–11159 (1979).
17. Allas, U., Liiv, A. & Remme, J. Functional interaction between RNase III and the *Escherichia coli* ribosome. *BMC Mol. Biol.* **4**, 8 (2003).
18. Li, Z. & Deutscher, M.P. RNase E plays an essential role in the maturation of *Escherichia coli* tRNA precursors. *RNA* **8**, 97–109 (2002).
19. Li, Z. & Deutscher, M.P. The role of individual exoribonucleases in processing at the 3′ end of *Escherichia coli* tRNA precursors. *J. Biol. Chem.* **269**, 6064–6071 (1994).
20. Zuo, Y. & Deutscher, M.P. Mechanism of action of RNase T. I. Identification of residues required for catalysis, substrate binding, and dimerization. *J. Biol. Chem.* **277**, 50155–50159 (2002).
21. Zuo, Y. & Deutscher, M.P. Mechanism of action of RNase T. II. A structural and functional model of the enzyme. *J. Biol. Chem.* **277**, 50160–50164 (2002).
22. Zuo, Y. *et al.* Crystal structure of RNase T, an exoribonuclease involved in tRNA maturation and end turnover. *Structure* **15**, 417–428 (2007).
23. Zuo, Y. & Deutscher, M.P. The DNase activity of RNase T and its application to DNA cloning. *Nucleic Acids Res.* **27**, 4077–4082 (1999).
24. Viswanathan, M., Dower, K.W. & Lovett, S.T. Identification of a potent DNase activity associated with RNase T of *Escherichia coli*. *J. Biol. Chem.* **273**, 35126–35131 (1998).
25. Zuo, Y. & Deutscher, M.P. The physiological role of RNase T can be explained by its unusual substrate specificity. *J. Biol. Chem.* **277**, 29654–29661 (2002).
26. Zuo, Y., Wang, Y. & Malhotra, A. Crystal structure of *Escherichia coli* RNase D, an exoribonuclease involved in structured RNA processing. *Structure* **13**, 973–984 (2005).
27. Chin, K.H., Yang, C.Y., Chou, C.C., Wang, A.H. & Chou, S.H. The crystal structure of XC847 from *Xanthomonas campestris*: a 3′-5′ oligoribonuclease of DnaQ fold family with a novel opposingly shifted helix. *Proteins* **65**, 1036–1040 (2006).
28. de Silva, U. *et al.* The crystal structure of TREX1 explains the 3′ nucleotide specificity and reveals a polyproline II helix for protein partnering. *J. Biol. Chem.* **282**, 10537–10543 (2007).
29. Jones, S., Daley, D.T., Luscombe, N.M., Berman, H.M. & Thornton, J.M. Protein-RNA interactions: a structural analysis. *Nucleic Acids Res.* **29**, 943–954 (2001).
30. Luscombe, N.M., Laskowski, R.A. & Thornton, J.M. Amino acid-base interactions: a three-dimensional analysis of protein-DNA interactions at an atomic level. *Nucleic Acids Res.* **29**, 2860–2874 (2001).
31. Ellis, J.J., Broom, M. & Jones, S. Protein–RNA Interactions: Structural analysis and functional classes. *Proteins.* **66**, 903–911 (2007).
32. Lavery, R., Moakher, M., Maddocks, J.H., Petkeviciute, D. & Zakrzewska, K. Conformational analysis of nucleic acids revisited: Curves+. *Nucleic Acids Res.* **37**, 5917–5929 (2009).
33. Cormack, R.S. & Mackie, G.A. Structural requirements for the processing of *Escherichia coli* 5S ribosomal RNA by RNase E in vitro. *J. Mol. Biol.* **228**, 1078–1090 (1992).
34. Ehretsmann, C.P., Carpousis, A.J. & Krisch, H.M. Specificity of *Escherichia coli* endoribonuclease RNase E: in vivo and in vitro analysis of mutants in a bacteriophage T4 mRNA processing site. *Genes Dev.* **6**, 149–159 (1992).
35. Deutscher, M.P. Ribonucleases, tRNA nucleotidyltransferase, and the 3′ processing of tRNA. *Prog. Nucleic Acid Res. Mol. Biol.* **39**, 209–240 (1990).
36. Dupasquier, M., Kim, S., Halkidis, K., Gamper, H. & Hou, Y.M. tRNA integrity is a prerequisite for rapid CCA addition: implication for quality control. *J. Mol. Biol.* **379**, 579–588 (2008).
37. Hartmann, R.K., Gossringer, M., Spath, B., Fischer, S. & Marchfelder, A. The making of tRNAs and more—RNase P and tRNase Z. *Prog. Mol. Biol. Transl. Sci.* **85**, 319–368 (2009).
38. Guerrier-Takada, C. & Altman, S. Catalytic activity of an RNA molecule prepared by transcription in vitro. *Science* **223**, 285–286 (1984).
39. Guerrier-Takada, C. & Altman, S. M1 RNA with large terminal deletions retains its catalytic activity. *Cell* **45**, 177–183 (1986).
40. Lehtinen, D.A., Harvey, S., Mulcahy, M.J., Hollis, T. & Perrino, F.W. The TREX1 double-stranded DNA degradation activity is defective in dominant mutations associated with autoimmune disease. *J. Biol. Chem.* **283**, 31649–31656 (2008).
41. Padmanabha, K.P. & Deutscher, M.P. RNase T affects *Escherichia coli* growth and recovery from metabolic stress. *J. Bacteriol.* **173**, 1376–1381 (1991).
42. Perry, J.J.P. *et al.* WRN exonuclease structure and molecular mechanism imply an editing role in DNA end processing. *Nat. Struct. Mol. Biol.* **13**, 414–422 (2006).
43. Yang, Y.G., Lindahl, T. & Barnes, D.E. Trex1 exonuclease degrades ssDNA to prevent chronic checkpoint activation and autoimmune disease. *Cell* **131**, 873–886 (2007).
44. Lee-Kirsch, M.A. *et al.* Mutations in the gene encoding the 3′-5′ DNA exonuclease TREX1 are associated with systemic lupus erythematosus. *Nat. Genet.* **39**, 1065–1067 (2007).
45. Riggs, A.D., Bourgeois, S., Newby, R.F. & Cohn, M. DNA binding of the lac repressor. *J. Mol. Biol.* **34**, 365–368 (1968).
46. Baba, T. *et al.* Construction of *Escherichia coli* K-12 in-frame, single-gene knockout mutants: the Keio collection. *Mol. Syst. Biol.* **2**, 2006–2008 (2006).

Acknowledgments

This work was supported by research grants from Academia Sinica and the National Science Council, Taiwan. Portions of this research were carried out at the National Synchrotron Radiation Research Center (BL-13B1 and BL-13C1), a national user facility supported by the National Science Council of Taiwan. The Synchrotron Radiation Protein Crystallography Facility is supported by the National Research Program for Genomic Medicine. We thank S. Lin-Chao (Academia Sinica) for providing the *E. coli* knockout strains used in this study.

Author contributions

Y.-Y.H. and H.S.Y. designed experiments and analyzed data. Y.-Y.H., C.-C.Y., C.L.L., J.L.J.L. and Y.D. carried out biochemical and structural analysis.

Competing financial interests

The authors declare no competing financial interests.

Additional information

Supplementary information is available online at http://www.nature.com/naturechemicalbiology/. Reprints and permissions information is available online at http://npg.nature.com/reprintsandpermissions/. Correspondence and requests for materials should be addressed to H.S.Y.